PCCP

Accepted Manuscript

ROYAL SOCIETY OF CHEMISTRY

www.rsc.org/pccp

Efficient Control of Coulomb Enhanced Second Harmonic Generation from Excitonic Transitions in Quantum Dot Ensembles

Hanz Y. Ramírez,[1,2,*] Jefferson Flórez,[3] and Ángela S. Camacho[4]

[1] *Grupo de Física Teórica y Computacional, Escuela de Física, Universidad Pedagógica y Tecnológica de Colombia (UPTC), Tunja 150003, Colombia.*

[2] *Division of Quantum Physics and Quantum Information, Hefei National Laboratory for Physics at the Microscale, University of Science and Technology of China, Hefei, Anhui 230026, China.*

[3] *Laboratorio de Óptica Cuántica, Universidad de los Andes, Bogotá D.C. 111711, Colombia.*

[4] *Departmento de Física, Universidad de los Andes, Bogotá D.C. 111711, Colombia.*

(Dated: August 8, 2015)

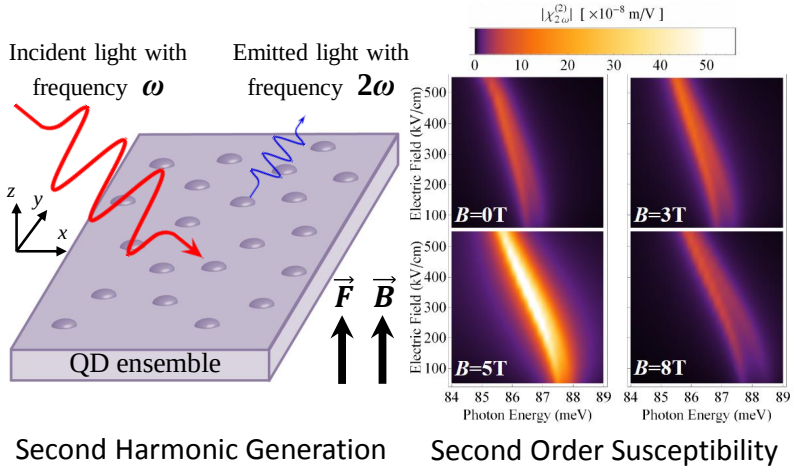

FIG. 0: Tunability and modulation of the second harmonic generation susceptibility, promising for manipulation of nonlinear properties of nanostructured materials, are predicted in this work.

Abstract

In this work, the second harmonic generation from excitonic transitions in semiconductor quantum dots is computationally studied. By integrating a density matrix treatment with a partial configuration interaction approach, we obtain for highly confined neutral and charged excitons, the second order susceptibility as function of externally applied electric and magnetic fields. Our results show enhancement in the nonlinear response respect to analogous optical processes based on intraband transitions, and predict its efficient tunability by taking advantage of the interplay between Coulomb effects and field-driven wave function manipulation.

PACS numbers: 78.67.Hc, 78.60.Lc, 42.70.Nq, 73.21.La

*Electronic address: hanz.ramirez@uptc.edu.co

I. INTRODUCTION

Nonlinear optical properties of low dimensional systems has become an interesting field of research because these nanostructures promise higher performance than other nonlinear materials such as polar crystals and organic polymers.[1, 2] When this is combined with some peculiar features of quantum dots, for instance the possibility of engineering carrier wave function by means of externally applied fields, the potential applications of their improved and controllable nonlinear optical characteristics can be diverse and remarkable.

Specifically, second harmonic generation (SHG) has been found useful in a wide range of applications including entanglement generation,[3, 4] determination of microscopic orientations,[5–7] bioimaging,[8, 9] and surface characterization.[10, 11]

However, absence of dipole moments for transitions between states of the same parity inhibits SHG in centrosymmetric structures.[12–14] Then, here we propose to take advantage of the trade-off between symmetry breaking and state intermixing generated by external fields and Coulomb interaction, respectively, to overcome such a limitation. This represents a possibility for induction and manipulation of second order nonlinearities in low-polar or non-polar systems.

Many works have previously considered SHG in zero dimensional systems, generally finding better optical nonlinearities than those observed in structures of higher dimensionality.[13, 15] In particular Brunhes et al. in Ref. [16], calculated and measured SHG susceptibilities for intraband transitions finding two main features: Good agreement of the experimental results with the predicted values obtained through a density matrix treatment of the nonlinear optical response, and surprisingly large values for these nonlinearities.

Following up, some studies on the matter have consistently found nonlinear optical intensities several orders of magnitude greater than those in bulk materials depending on geometrical and strain effects; although these studies dismissed the Coulomb interaction in strongly confined nanostructures under the argument of its much lower typical energy scale.[17–23]

Further on, several works have called the attention on the relevance of electrostatic effects on the nonlinear response of low dimensional systems, [24–28] thus stressing the importance of including the Coulomb impact on the modeling of those kind of optical processes.

In this work we study the SHG from exciton transitions in quantum dot ensembles, and

show how manipulation of the Coulomb interaction through applied fields and/or carrier injection, both of them external and post fabrication control mechanisms, [29–31] allows for efficient modulation of this second order susceptibility in the strongly confined regime. Such a result represents a significant contribution towards all-tunable nonlinear materials.

This paper is organized as follows. Section II presents the models used in describing the nonlinear optical response and the confined excitons in quantum dots. The application of a time independent electric field, inclusion of the Coulomb interaction, and their competing interplay are shown and discussed in section III and IV. Section V reports the effects of applying a magnetic field, and finally the influence of additional charge in an exciton complex is addressed in section VI. Section VII provides a summary and conclusions.

II. THEORETICAL MODEL

In our approach to study nonlinearities of quantum dot ensembles, two main components are to be integrated. On one hand the model to establish the strength of the nonlinear optical response to the stimulating light in a collective of nanostructures with fully discretized energy levels. On the other hand the particular description at the single dot level of the transition energies and dipole moments that are involved in the modeled optical process.

A. Optical model

The light-matter interaction is here studied using the density matrix formalism, which allows in a very convenient way to introduce decoherence effects in the calculation of the susceptibility.[32, 33]

We will assume quantum dot size homogeneity along the ensemble, which in despite of being an idealization of the system is a reasonable approximation considering the continuous improvements in the growth techniques and the significant simplification that it allows in the calculations.

The equation of motion for $\hat{\rho}$ is

$$\frac{\partial \rho_{ij}}{\partial t} = \frac{1}{i\hbar}[\hat{H}_0 + \hat{H}', \hat{\rho}]_{ij} - \Gamma_{ij}(\rho_{ij} - \rho_{ij}^{(0)}), \tag{1}$$

where $\hat{\rho}^{(0)}$ is the density matrix operator for the non-interacting system at thermal equi-

librium, and $\Gamma_{ii} = T_1^{-1}$ $(i = j)$ and $\Gamma_{ij} = T_2^{-1}$ $(i \neq j)$ are decoherence rates which absorb size inhomogeneities along the sample as well as relaxation and dephasing processes.[16, 34] $\hat{H}_0$ is taken to be the time independent part of the Hamiltonian, so that $\mid i\rangle$ and E_i are the corresponding eigenstates and eigenvalues satisfying $\hat{H}_0 \mid i\rangle = E_i \mid i\rangle$, while $\hat{H}'$ is the time dependent part of the Hamiltonian which describes the light-matter coupling.

Given that the wavelength of the stimulating radiation is around three orders of magnitude larger than the average quantum dot constituting the artificial gas, the dipole approximation is used, [35, 36] and $\hat{H}'$ becomes

$$\hat{H}' = -\mathrm{e}\hat{z}\mathcal{E}(t), \tag{2}$$

where $\mathrm{e} > 0$ is the electron charge and $\mathcal{E}(t) = \tilde{\mathcal{E}}(\omega)e^{i\omega t} + \text{c.c.}$ is the electric field of the incident electromagnetic wave, assumed here to be polarized along the z-axis.

Equation (1) is solved iteratively using the expansion

$$\hat{\rho} = \hat{\rho}^{(0)} + \hat{\rho}^{(1)} + \hat{\rho}^{(2)} + \cdots \ . \tag{3}$$

This expansion inserted into equation (1) allows us to calculate the induced second order polarization (and then $\chi^{(2)}$) as the ensemble average

$$\langle \hat{P}^{(2)} \rangle = \mathrm{Tr}\left(\hat{\rho}^{(2)}\hat{P}\right) \ . \tag{4}$$

with $\hat{P} = n_0 e\hat{z}$ and n_0 the three-dimensional quantum dot density.

Keeping only the double-frequency contribution to the second order polarization, which originates the well known SHG process, and defining $\chi^{(2)}_{2\omega}(\omega) = \langle \hat{P}^{(2)}_{2\omega} \rangle / \varepsilon_0 \tilde{\mathcal{E}}^2(\omega)$ as the second order susceptibility for the SHG process, for a three-level system one obtains

$$\chi^{(2)}_{2\omega}(\omega) = \frac{n_0 \mathrm{e}^3 \rho^{(0)}_{11}}{\varepsilon_0 \hbar^2} \frac{z_{12} z_{23} z_{31}}{(2\omega - \omega_{31} - i\Gamma_{13})(\omega - \omega_{21} - i\Gamma_{12})} \ . \tag{5}$$

Thus, the magnitude of this nonlinear response can be calculated in terms of the dipole moments $z_{ij} \equiv \langle i \mid \hat{z} \mid j \rangle$ $(i, j = 1, 2, 3)$, and of the transition energies $\hbar\omega_{21}$ and $\hbar\omega_{31}$.[32]

B. Quantum dot model

The constituting unit of the ensemble (single quantum dot) is modeled by an axially symmetric 3D harmonic confinement potential for each carrier. In contrast with other studies, we allow different confining frequencies for the electron and hole, which is much more appropriate considering the differences in the offsets and effective masses between the valence and conduction bands.[37, 38]

Under this confinement, the single particle (electron or hole) Hamiltonian reads

$$\hat{H}^{e/h} = -\frac{\nabla^2}{2m^*_{e/h}} + \frac{m^*_{e/h}(\omega_r^{e/h})^2(x^2_{e/h}+y^2_{e/h})}{2} + \frac{m^*_{e/h}(\omega_z^{e/h})^2 z^2_{e/h}}{2} \ , \tag{6}$$

where $m^*_{e/h}$ is the electron/hole effective mass, and $\omega_r^{e/h}$ ($\omega_z^{e/h}$) the electron/hole frequency associated to the harmonic in-plane (vertical) confinement.

Eigenstates of the Hamiltonians in equation (6), are the familiar Fock-Darwin states $\Phi^{e/h}_{i^{e/h}}$; where the electron/hole label $i^{e/h}$ is an index composed by the three quantum numbers $n^{e/h}$, $m^{e/h}$, and $q^{e/h}$. These first two numbers correspond to in-plane excitations, while the third one refers to the z direction.

Focusing on the single particle ground states $n^{e/h} = m^{e/h} = q^{e/h} = 0$, the corresponding wave functions have characteristic extents directly related to the confining frequencies according to

$$l_r^{e/h} = \sqrt{\frac{\hbar}{2m^*_{e/h}\omega_r^{e/h}}} \quad , \quad l_z^{e/h} = \sqrt{\frac{\hbar}{2m^*_{e/h}\omega_z^{e/h}}} \ . \tag{7}$$

In real quantum dots, the electron parameters are usually larger than those of the hole. Although the main features of the nonlinear response are not substantially affected by it, in this work we consider e-h asymmetry indexes of $\frac{l_z^h}{l_z^e} = 0.5$ and $\frac{l_r^h}{l_r^e} = 0.75$.[39]

Because of such an asymmetry, it is convenient to define the hybridized e-h wave function parameters

$$l_r^{eh} \equiv \sqrt{\frac{(l_r^e)^2+(l_r^h)^2}{2}} \quad , \quad l_z^{eh} \equiv \sqrt{\frac{(l_z^e)^2+(l_z^h)^2}{2}} \ , \tag{8}$$

based on which the quantum dot aspect ratio can be defined as $a \equiv \frac{l_z^{eh}}{l_r^{eh}}$.

Regarding energies, the single particle eigenvalues are given by

$$E^{e/h}_{n^{e/h},m^{e/h},q^{e/h}} = \hbar\omega_r^{e/h}(n^{e/h} + m_e^{e/h} + 1) + \hbar\omega_z^{e/h}(q_e^{e/h} + \frac{1}{2}) \ . \tag{9}$$

It is important to note than within this model, existence of electron-hole pairs in the ensemble is assumed, which can be achieved by means of optical pumping on the sample. Regarding dynamic control of the nonlinear response,[40, 41] this actually represents an advantage of such interband scheme as compared to intraband systems where the presence of confined carriers in the quantum dot ensemble is achieved by conventional doping. Furthermore if compared to systems where population is controlled by gate voltages,[42] this optically activated occupation of the dots seems still more efficient and deterministic, because using voltages to depopulate may require very strong fields to deplete deeply bound states (far below the band offset).

III. ELECTRIC FIELD EFFECTS

Although self-assembled dots generally exhibit some asymmetry along the growth direction, in this study vertically centrosymmetric structures are considered. This means to evaluate the Coulomb and field effects in the worst scenario for nonlinearities, because as described by equation (5), non-zero transition dipole moments are required in the polarization direction to observe SHG. Thus, since the ignored asymmetries would contribute to the transition dipole moments, the SHG susceptibilities calculated in what follows would be even larger, and the enhancement in their magnitudes respect to those of intraband transitions should be even more substantial.

In those vertically symmetric quantum dots, occurrence of non-vanishing dipole moments requires a symmetry breaking which in our model is achieved and controlled by applying a bias field.[43, 44]

The corresponding term in the Hamiltonian reads

$$\hat{H}^{bf} = \mid \mathrm{e} \mid F \ (z_e - z_h) \quad , \tag{10}$$

where F is the magnitude of a time independent bias applied in the z direction.

When added to the non-interacting e-h part of the Hamiltonian in equation (6), the bias term shifts the origins of the harmonic confinements in the growth direction, by quantities with units of length linearly depending on F equal to

$$\beta_{e/h} \equiv -/+ \ \mathrm{e} \ F \ \frac{1}{m^*_{e/h}(\omega_z^{e/h})^2} \ , \tag{11}$$

and introduces an energy offset given by

$$E_{bf} = \frac{(\mathrm{e}F)^2}{2}\left(\frac{1}{m^*_h(\omega_z^h)^2} - \frac{1}{m^*_e(\omega_z^e)^2}\right) \ . \tag{12}$$

The distance $\beta = \mid \beta_e - \beta_h \mid$ represents the bias-driven separation between electron and hole, which simultaneously accounts for reduction in the Coulomb interaction and increase in the dipole moments.

IV. COULOMB EFFECTS

Spin influence is neglected in this work, given that the g-factor of heterostructures made of wide bandgap materials is known to be small,[45–48] and also because the magnitude of the e-h exchange energy is normally much smaller than the exciton direct and correlation Coulomb interactions, whose effects are the main scope of this work.[39, 49, 50] Thus, the complete time independent Hamiltonian reads

$$\hat{H}^T = \hat{H}^e + \hat{H}^h + \hat{H}^{bf} + \hat{H}^{eh} \ , \tag{13}$$

in which, along with the single particle and bias terms, the e-h Coulomb interaction is included. Such a term explicitly reads

$$\hat{H}^{eh} = -\sum_{n,j,k,m} V^{eh}_{n,j,k,m} h^\dagger_n c^\dagger_j c_k h_m \ , \tag{14}$$

where $h^\dagger$ and $c^\dagger$ (h and c) are the electron and hole creation (annihilation) operators, respectively. The corresponding matrix elements are given by

$$\hat{H}^{eh} = \int\int d^{(3)}\vec{r}_e \; d^{(3)}\vec{r}_h \; \Phi_n^{h*}(\vec{r}_h)\Phi_j^{e*}(\vec{r}_e) \times \frac{e^2}{4\pi\varepsilon_0\varepsilon \mid \vec{r}_e - \vec{r}_h \mid}\Phi_k^e(\vec{r}_e)\Phi_m^h(\vec{r}_h) \; . \tag{15}$$

With the purpose of characterizing the magnitude of the Coulomb interaction and its effects, we carry out calculations for obtaining eigenenergies at three levels of approximation: Non-interacting e-h, first order perturbation, and configuration interaction (CI). In the last case S, P, and D-like single particle orbitals are considered.

To find the eigenenergies within each of the chosen approaches, we either suppress all interaction terms, keep only diagonal Coulomb terms, or include both diagonal and off-diagonal terms, respectively.

Therefore in the CI calculation, by diagonalizing the Hamiltonian of equation (13) written in the basis defined by the direct product of $\hat{H}^e$ and $\hat{H}^h$ eigenstates, the eigenenergies and envelope wave functions of the confined exciton are acquired.

To obtain the bias dependent e-h Coulomb matrix elements, we add a label i or f to electron and hole quantum numbers depending on their association to the initial or final transition state, and extend the result by Chen et al. in Ref. [48] so that holes and bias effects can be incorporated. Thus, for the considered dots of aspect ratio $a \leq 1$ we use

$$\begin{aligned}
&\langle n_f^e, m_f^e, q_f^e \mid n_f^h, m_f^h, q_f^h \mid H^{e-h} \mid n_i^h, m_i^h, q_i^h \mid n_i^e, m_i^e, q_i^e \rangle = \\
&-\frac{\mathrm{e}^2 e^{-\frac{\beta^2}{4(l_z^{eh})^2}}}{8\pi^2\varepsilon_0\varepsilon l_r^{eh}} \frac{\delta_{L_f,L_i} \;\; \delta_{q_f^e+q_f^h+q_i^h+q_i^e,\text{even}}}{\sqrt{n_f^e!m_f^e!q_f^e!n_f^h!m_f^h!q_f^h!n_i^h!m_i^h!q_i^h!n_i^e!m_i^e!q_i^e!}} \\
&\times \sum_{p_1=0}^{\min(n_f^e,n_i^e)} \sum_{p_2=0}^{\min(m_f^e,m_i^e)} \sum_{p_3=0}^{\min(q_f^e,q_i^e)} \sum_{p_4=0}^{\min(n_f^h,n_i^h)} \sum_{p_5=0}^{\min(m_f^h,m_i^h)} \sum_{p_6=0}^{\min(q_f^h,q_i^h)} p_1!p_2!p_3!p_4!p_5!p_6! \\
&\times \binom{n_f^e}{p_1}\binom{n_i^e}{p_1}\binom{m_f^e}{p_2}\binom{m_i^e}{p_2}\binom{q_f^e}{p_3}\binom{q_i^e}{p_3}\binom{n_f^h}{p_4}\binom{n_i^h}{p_4}\binom{m_f^h}{p_5}\binom{m_i^h}{p_5}\binom{q_f^h}{p_6}\binom{q_i^h}{p_6} \\
&(-1)^{u+n_f^h+m_f^h+q_f^h+n_i^h+m_i^h+q_i^h+\frac{v}{2}} \left(\frac{1}{2}\right)^u \left(\frac{(l_z^{eh})^2}{(l_r^{eh})^2}\right)^{\frac{v}{2}} \frac{\Gamma\left(\frac{1+2u+v}{2}\right)\Gamma\left(1+u\right)\Gamma\left(\frac{1+v}{2}\right)}{\Gamma\left(\frac{3+2u+v}{2}\right)} \\
&{}_2F_1\left(\frac{1+v}{2}, \frac{1+2u+v}{2}, \frac{3+2u+v}{2}, 1-\left(\frac{(l_z^{eh})^2}{(l_r^{eh})^2}\right)\right) \; ,
\end{aligned} \tag{16}$$

where $u \equiv m_i^e + m_f^h + n_f^e + n_i^h - (p_1 + p_2 + p_4 + p_5)$ and $v \equiv q_f^e + q_f^h + q_i^e + q_i^h - 2p_3 - 2p_6$. $\Gamma(x_1)$ and ${}_2F_1(x_1, x_2, x_3, x_4)$ represent the Euler Gamma and Hypergeometric ${}_2F_1$ functions,

respectively. $\delta_{q_f^e+q_f^h+q_i^h+q_i^e,\text{even}}$ preserves vertical parity, while δ_{L_i,L_f} ensures conservation of the z component of angular momentum, being $L_i \equiv (n_i^e - m_i^e) + (m_i^h - n_i^h)$ and $L_f \equiv (n_f^e - m_f^e) + (m_f^h - n_f^h)$.

Figure 1(a) illustrates the studied system, in which a neutral exciton (X^0) is confined in an axially symmetric quantum dot under action of the electric field $\vec{F}$.

In order to evaluate Coulomb effects, the relative energy differences $\Delta E^i_{UP;CI} \equiv | \frac{E^i_{CI}-E^i_{UP}}{E^i_{CI}} |$ and $\Delta E^i_{PT;CI} \equiv | \frac{E^i_{CI}-E^i_{PT}}{E^i_{CI}} |$ are defined for the ith eigenstate, where E^i_{UP}, E^i_{PT}, and E^i_{CI} are the corresponding eigenenergies obtained by the non-interacting, first order perturbation, and CI approach, respectively. Thus, taking the CI calculation as reference, $\Delta E^i_{UP;CI}$ measures the composed influence of direct and indirect Coulomb terms, while $\Delta E^i_{PT;CI}$ accounts only for the indirect ones (correlations).

In what follows, some specific material parameters have to be chosen in order to carry out numerical simulations that elucidate the wanted Coulomb effects. In this case, InGaAs/GaAs dots are considered and close dependence between such particular parameters and the obtained magnitudes must be taken into mind.[51] Nevertheless, the assumptions behind this approach allow to extrapolate the observed trends to a wide range of III-V or even II-VI direct-gap semiconductor dot samples, since the studied underlying physics is in principle common to all of them. Moreover, it could be expected that the more polar the considered material (e.g. CdTe dots), the stronger the enhancement effect.[13]

Figure 1(b) shows those relative energy differences as functions of the applied bias field. The expected reduction of the Coulomb interaction for stronger fields is verified, and the tiny influence of correlations on eigenenergies is evidenced. It is also consistent with the known fact that electrostatic effects are more noticeable on the ground energy than on excited levels.[27, 52]

The norm of the second harmonic generation susceptibility (SHGS) $| \chi^{(2)}_{2\omega} |$, is plotted in figure 2(a) as a function of the stimulating photon energy and the bias field.[53] In figure 2(b), the SHGS is shown as a function of the stimulating photon energy for some chosen bias values.

As it can be noted in equation (5), the SHGS has two distinctive peaks in $\hbar\omega = E_2 - E_1$ and $2\hbar\omega = E_3 - E_1$, being the later larger than the first one within this model because $2(E_2 - E_1) > (E_3 - E_1)$. Without Coulomb effects, the harmonic exciton confinement implies $2(E_2 - E_1) = (E_3 - E_1)$, which would produce the so-called double resonance condition

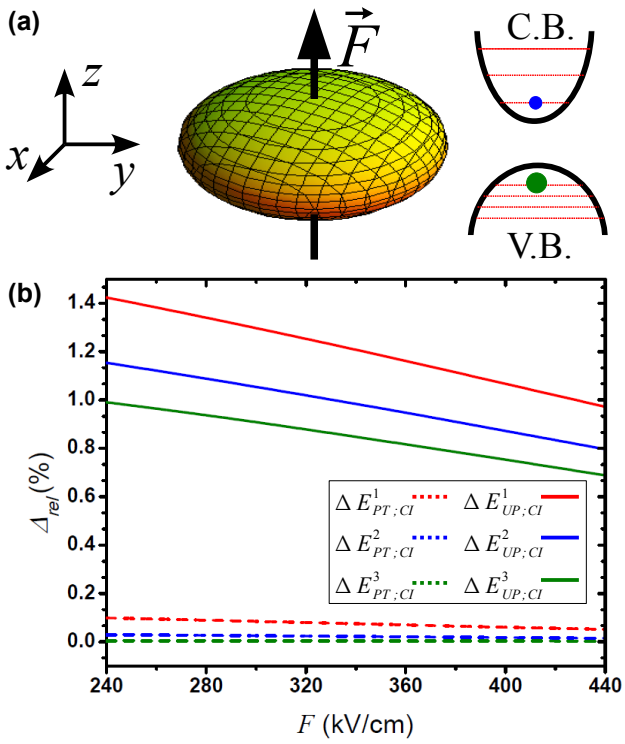

FIG. 1: (a) Schematics of the artificial atom where a neutral exciton is confined. (b) Direct Coulomb and correlation effects on the three lowest eigenenergies.

(DRC).[54] Strong bias fields lead the system to recover the DRC by weakening the Coulomb interaction between electron and hole.

Having into account that because of well-defined parity of the single carrier wave functions, Coulomb related state intermixing is required to obtain non vanishing z_{31} dipole moment within our model; it is interesting to observe the interplay between the bias-related enhanced asymmetry and the reduced Coulomb interaction, so that the system reaches a SHGS maximum at some electric field value. Such an optimization is clearly evidenced in figure 2(b).

The red-shift with increasing bias can be understood in terms of the reduction in the push-down Coulomb effect experienced by the ground state.

For the sake of verification of the order of magnitude obtained for the maximum, those computed SHGS may be collated with the ones shown in figure 8 of reference,[16] being aware that resonant conditions and vertical confinement asymmetry are dissimilar in both works.[55] In doing that, our results are found at the same order of magnitude as the experimental

ones reported there, and one order of magnitude larger than their theoretical prediction. This leads us to think that the discrepancy between experimental and theoretical results in that work, might be attributed to the disregarding of the Coulomb interaction, which must be somehow present given that the calculation parameters used there reflect a number of carriers 1.5 times the number of dots, thus making the average occupation larger than 1. If Coulomb effects would be considered, external stationary fields would also play an interesting role in that kind of intraband system.

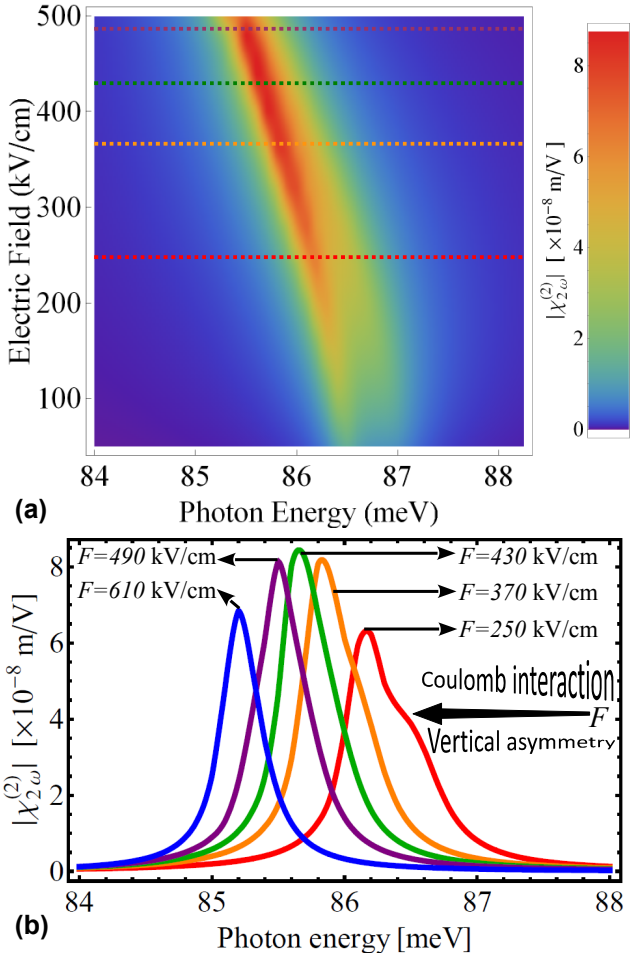

FIG. 2: (a) Norm of the SHG susceptibility as function of the stimulating frequency and the bias field. (b) Profile of the SHG susceptibility as function of the stimulating frequency for some specific values of F [four of the five chosen fields are highlighted in (a)]

V. MAGNETIC FIELD EFFECTS

Pursuing additional control on the nonlinear response, we added a time independent magnetic field to the system. To do that, it is necessary to change the canonical momentum operator $-\frac{\nabla^2}{2m^*_{e/h}}$ by the kinematical one $-\frac{\nabla^2}{2m^*_{e/h}} \pm \mid \mathrm{e} \mid \boldsymbol{A}(\boldsymbol{r}_{e/h})$, where $\boldsymbol{A}(\boldsymbol{r}_{e/h}) = \frac{B}{2}(-y_{e/h}, x_{e/h}, 0)$ is the magnetic potential taken in the Coulomb gauge.[52] This results in modifications of the electron and hole harmonic frequencies according to

$$\omega^{e/h}_{r,B} = \sqrt{(\omega^{e/h}_r)^2 + \left(\frac{\omega^{e/h}_c}{2}\right)^2} \ , \tag{17}$$

where $\omega^{e/h}_c = \mp\frac{eB}{m^*_{e/h}}$ is the corresponding cyclotron frequency.

Because of axial symmetry, it is convenient to define the chiral frequencies

$$\omega^{e/h}_{\pm} = \left(\omega^{e/h}_{r,B} \pm \omega^{e/h}_c\right) \ , \tag{18}$$

so that the single particle energies depending on the magnetic field, are given by

$$E^{e/h}_{n,m,q}(B) = \hbar\omega^{e/h}_{+}(n_e + \frac{1}{2}) + \hbar\omega^{e/h}_{-}(m_e + \frac{1}{2}) + \hbar\omega^{e/h}_{z}(q_e + \frac{1}{2}) \ . \tag{19}$$

Markedly, the magnetic field affects the exciton in two ways: First, it shrinks the electron and hole wave functions, magnifying the Coulomb matrix elements. Second, it shifts the in-plane contributions to the single particle energies, modifying the energy distance between different exciton states.

The SHGS as function of both of the stimulating photon energy and the bias field, is shown in figure 3 for different magnetic field values. There, the additional possibility of modulation gained by applying magnetic field can be appreciated. Improvement of the SHGS in a factor of around 5 is observed when a magnetic field of 5 T is turned on, which is directly related to strengthened Coulomb effects.

However, the growing trend is not monotonic as can be observed for a field of 8 T. Under that field, the calculated SHGS is even smaller than that when no magnetic field was applied. This evidences that larger Coulomb matrix elements are not the only necessary thing for increasing the nonlinear response.

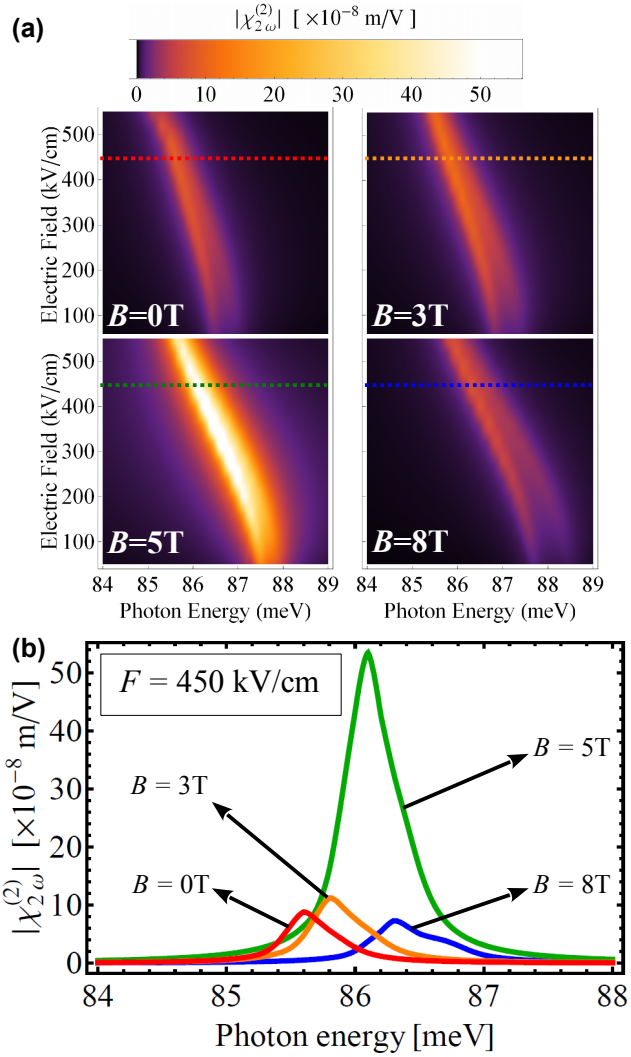

FIG. 3: (a) Norm of the SHG susceptibility as a function of the stimulating frequency and the bias field, for different magnetic field values. (b) Comparison at F =450 kV/cm of the norm of the SHG susceptibility for different magnetic field values.

Figure 4 provides some enlightening information for understanding the modulated behavior. We use $V_{eh} = \langle 0,0,0,0,0,0 \mid H^{e-h} \mid 0,0,0,0,0,0 \rangle$ (the main direct Coulomb matrix element), to get an estimation of the interaction magnitude. In figure 4(a) the competition between vertical asymmetry and electrostatic interaction is elucidated, and the increase of the Coulomb matrix elements with the magnetic field is manifested. Figure 4(b) shows the product of the involved dipole moments as a function of the bias field for different magnetic field values. The inset presents the eigenenergies of three particular states of the basis which contribute to state intermixing, and the corresponding indirect Coulomb

matrix elements. These states are $\mid E_A\rangle \equiv \mid 2,0,0 \mid 2,0,0\rangle$, $\mid E_B\rangle \equiv \mid 0,0,0 \mid 1,1,0\rangle$, and $\mid E_C\rangle \equiv \mid 0,1,0 \mid 0,1,0\rangle$; while the matrix elements are $V_{A,B} \equiv \langle E_A \mid H^{e-h} \mid E_B\rangle$, $V_{A,C} \equiv \langle E_A \mid H^{e-h} \mid E_C\rangle$, and $V_{B.C} \equiv \langle E_B \mid H^{e-h} \mid E_C\rangle$.

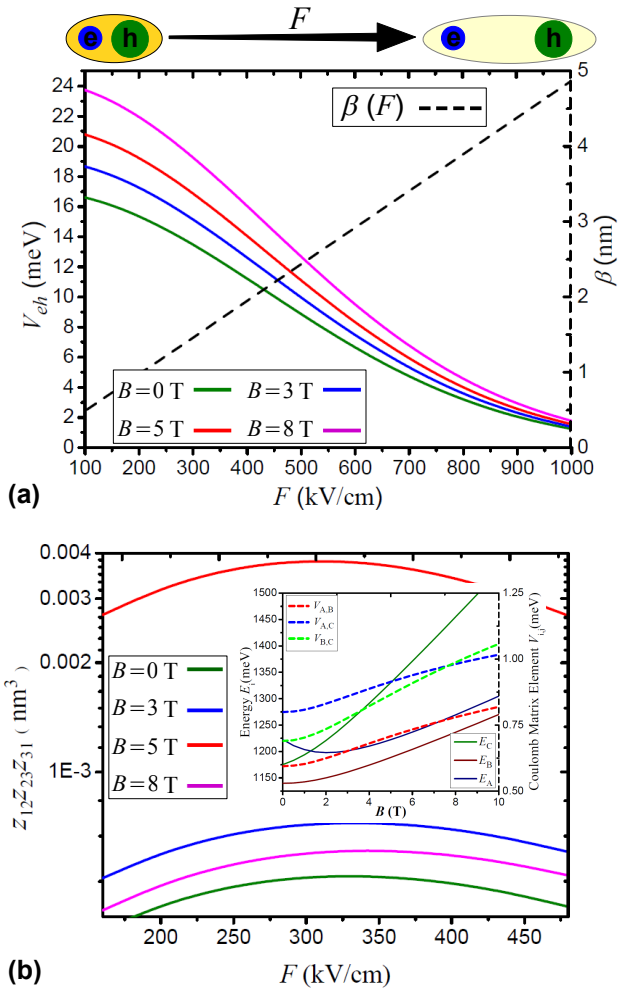

FIG. 4: (a) V_{eh} and β as functions of the bias field for different magnetic field values. (b) Dipole moment product $z_{12}z_{23}z_{31}$, calculated as a function of the bias field for different magnetic field values. The inset shows particular non interacting eigenenergies and the corresponding Coulomb matrix elements.

In the inset of figure 4(b), it is observed how the off-diagonal Coulomb matrix elements also grow with the magnetic filed. Nevertheless, the energy distance between the mixing states varies with field, making relative the influence of the enlarged matrix elements, given that hybridization of states depends not just on the magnitude of the mixing terms, but also on closeness of the involved states eigenenergies.[56]

It is worth mentioning that figures 4(a) and 4(b) evidence strong correlation between the magnitude of SHGS and the effectiveness of the Coulomb interaction in causing state intermixing. Indeed, calibration calculations carried out along this work, showed that if the e-h electrostatic interaction is artificially tended turned off, the dipole moment z_{31} vanishes even for very high bias fields.[44, 57, 58]

VI. CHARGED EXCITON

In the last part of this work, charge effects on the SHGS for an exciton complex are studied. We calculate the SHGS for a negatively charged exciton (X^-) as function of the bias field with and without magnetic field.

The modified systems is depicted in figure 5(a), where the additional considered electron is shown. The negatively charged exciton was chosen because in this configuration the Coulomb effects are expected to be potentiated because of the more extended spatial distribution of the electron wave function as compared to that of the hole.[59, 60]

The Coulomb interaction matrix elements for the three particle system $\langle f \mid \hat{H}^{Cou} \mid i\rangle$, are obtained according to

$$\begin{aligned}
&\langle n_f^{e2}, m_f^{e2}, q_f^{e2} \mid n_f^{e1}, m_f^{e1}, q_f^{e1} \mid n_f^h, m_f^h, q_f^h \mid H^{Cou} \mid n_i^h, m_i^h, q_i^h \mid n_i^{e1}, m_i^{e1}, q_i^{e1} \mid n_i^{e2}, m_i^{e2}, q_i^{e2}\rangle = \\
&-\langle n_f^{e2}, m_f^{e2}, q_f^{e2} \mid n_f^h, m_f^h, q_f^h \mid H^{e-h} \mid n_i^h, m_i^h, q_i^h \mid n_i^{e2}, m_i^{e2}, q_i^{e2}\rangle \ \delta_{n_f^{e1},n_i^{e1}}\delta_{m_f^{e1},m_i^{e1}}\delta_{q_f^{e1},q_i^{e1}} \\
&-\langle n_f^{e1}, m_f^{e1}, q_f^{e1} \mid n_f^h, m_f^h, q_f^h \mid H^{e-h} \mid n_i^h, m_i^h, q_i^h \mid n_i^{e1}, m_i^{e1}, q_i^{e1}\rangle \ \delta_{n_f^{e2},n_i^{e2}}\delta_{m_f^{e2},m_i^{e2}}\delta_{q_f^{e2},q_i^{e2}} \\
&+\langle n_f^{e2}, m_f^{e2}, q_f^{e2} \mid n_f^{e1}, m_f^{e1}, q_f^{e1} \mid H^{e-e} \mid n_i^{e1}, m_i^{e1}, q_i^{e1} \mid n_i^{e2}, m_i^{e2}, q_i^{e2}\rangle \ \delta_{n_f^h,n_i^h}\delta_{m_f^h,m_i^h}\delta_{q_f^h,q_i^h} \ , \quad (20)
\end{aligned}$$

where the labels $e1$ and $e2$ have been introduced referring to either of the two electrons. The expression of the matrix element for the e-e interaction is analogue to that for the e-h one, but differs in that the former does not depend on the bias field, and conservation of the z component of angular momentum is now given by $\delta_{L_i',L_f'}$ with $L_i' \equiv (m_i^{e1}+m_i^{e2})-(n_i^{e1}+n_i^{e2})$ and $L_f' \equiv (m_f^{e1}+m_f^{e2})-(n_f^{e1}+n_f^{e2})$.

In figure 5(b), the intensity of the direct and correlation Coulomb effects can be observed for the negatively charged exciton as functions of the bias field. Although the direct Coulomb effects are stronger in the X^0 case,[61] correlations which are the responsible of state intermixing are noticeably larger in the X^- case. The corresponding values for $B = 0$ are

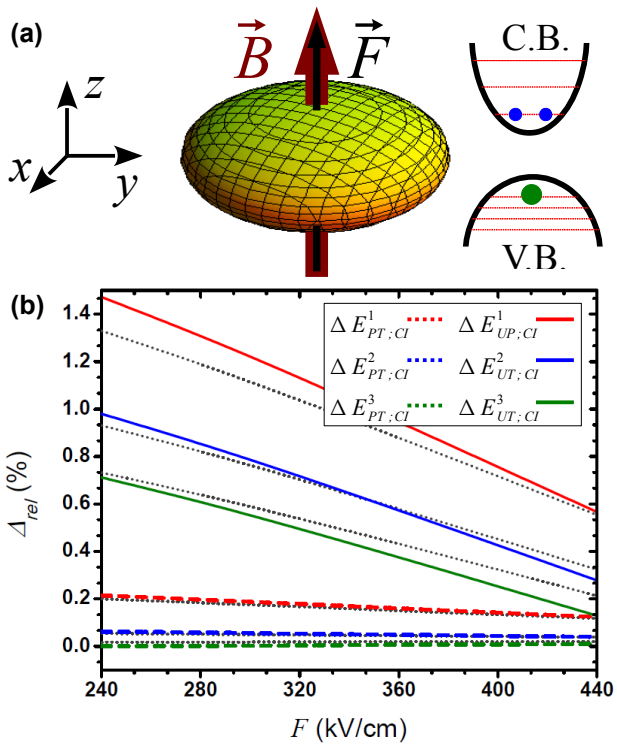

FIG. 5: (a) Schematics of the artificial atom where a negatively charged exciton is confined. (b) Direct Coulomb and correlation effects on the three lowest eigenenergies of the confined charged exciton under magnetic axial field B =5 T. The dashed black lines show the same percentages without magnetic field.

also shown in dashed lines, and allow to observe how the magnetically driven wave function shrinking, increases electrostatic interaction for lower bias fields but leads to faster reduction of the Coulomb influence for higher bias values.

The X^- SHGS as a function of the stimulating photon energy is shown in figure 6(a) for different bias values and are displayed in such a way that results can be directly compared with the corresponding X^0 case.

The SHGS improvement in around one order of magnitude is clear, and figure 6(b) evidences that the gain is rooted in the larger product of dipole moments for the charged exciton. This product is in turn favored by the Coulomb driven hybridization of states.

Defining the ratio $\frac{E_3-E_2}{E_2-E_1}$, which accounts for breaking of the DRC for each of the X^0 and X^- cases, the strength of the Coulomb related intermixing can be visualized (i. e. the farther this ratio is from 1, the stronger the mix of states), as done in the inset of figure

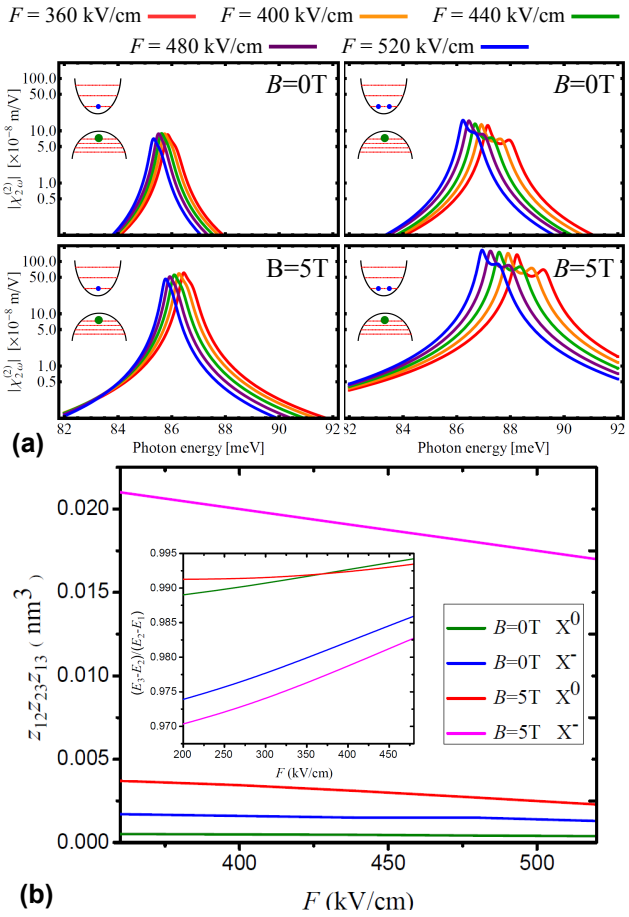

FIG. 6: (a) SHGS as function of the stimulating photon energy at different bias fields for X^0 and X^-. (b) Dipole moment product $z_{12}z_{23}z_{31}$, calculated as a function of the bias field for X^0 and X^-. The inset shows the ratio $\frac{E_3-E_2}{E_2-E_1}$ for the corresponding cases.

6(b). As presumed, stronger Coulomb effects in the charged exciton configuration enhance the nonlinear response of the system.

VII. SUMMARY AND CONCLUSIONS

In this work, manipulation of the Coulomb effects on the second harmonic generation from quantum dot ensembles was studied. Significant amplification and efficient control of the corresponding second order susceptibility under application of electric and magnetic external fields are predicted. Besides neutral excitons, further improvement of the nonlinear response was obtained for negatively charged excitons as compared to neutral excitons.

The magnitude of Coulomb matrix elements and their consequent state intermixing were

addressed as the underlaying mechanisms for efficient on-demand modulation and important gain in the maximum of the second harmonic resonance. Thus, interband setups are found superior to pure intraband schemes (in which no significant role is played by electrostatic interaction), for second harmonic generation and its associated applications.

Beyond pointing out the relevance of electrostatic interaction on nonlinear optical properties of quantum dot ensembles, it was demonstrated how all-external wave function control in zero dimensional systems leads to tunable nonlinearities via Coulomb correlations, in despite of their characteristic scale several orders of magnitude smaller than energy spacing due to quantum confinement.

Although these results were obtained for ensembles formed by identical dots, the inherent physics is anticipated to stand under moderate size inhomogeneities. Thus, the main predicted features should be susceptible of observation in real high quality artificial gases. This might represent a significant contribution toward nanostructured tunable nonlinear materials.

Acknowledgments

The authors acknowledge the UPTC's Research Division (project SGI 1761), the Department of Physics of the Universidad de Los Andes and the Chinese Academy of Sciences (grant no. 2011Y1JB03UP) for financial support.

[1] E. Rosencher, A. Fiore, B. Vinter, V. Berger, Ph. Bois, and J. Nagle, Science **1996**, *271*, 168.

[2] V. Gavrilenko and O. Aktsipetrov, *Nonlinear Optics of Surfaces and Nanostructures*, Wiley-Interscience, Hoboken NJ, USA **2014**, and references therein.

[3] N. B. Grosse, W. P. Bowen, K. McKenzie, and P. K. Lam, Phys. Rev. Lett. **. 2006**, *96*, 063601.

[4] N. B. Grosse, S. Assad, M. Mehmet, R. Schnabel, T. Symul, and P. K. Lam, Phys. Rev. Lett. **2008**, 100, 243601.

[5] W. T. Hsu, Z. A. Zhao, L. J. Li, C. H. Chen, M. H. Chiu, P. S. Chang, Y. C. Chou, and W. H. Chang, ACS Nano **2014**, *8*, 2951.

[6] J. I. Dadap and K. B. Eisenthal, J. Phys. Chem. B **2014**, *118*, 14366.

[7] H. B. Hu, K. Wang, H. Long, W. W. Liu, B. Wang, and P. X. Lu, Nano Lett. **2015**, *15*, 3351.

[8] J. E. Reeve, H. L. Anderson, and K. Clays, Phys. Chem. Chem. Phys. **2010**, *12*, 13484.

[9] L. Mayer, A. Slablab, G. Dantelle, V. Jacques, A. M. Lepagnol-Bestel, S. Perruchas, P. Spinicelli, A. Thomas, D. Chauvat, M. Simonneau, T. Gacoin, and J. F. Roch, Nanoscale **2013**, *5*, 8466.

[10] R. R. Kumal, T. E. Karam, and L. H. Haber, J. Phys. Chem. C **2015**, *119*, 16200.

[11] O. A. Castaeda-Urib, R. Reifenberger, A. Raman, and A. Avila, ACS Nano, **2015**, *9*, 2938.

[12] S. Sauvage, P. Boucaud, F. F. Glotin, R. Prazeres, J.-M. Ortega, F. A. Lemaître, J.-M. Gérard, and V. Thierry-Mieg, Phys. Rev. B **1999**, *59*, 9830.

[13] S. Winter, M. Zielinski, D. Chauvat, J. Zyss, and D. Oron, J. Phys. Chem. C 2011, 115, 4558.

[14] W. P. Dempsey, S. E. Fraser, and P. Pantazis, Bioessays **2012**, *34*, 351.

[15] O. S. Wolfbeis, : Chem. Soc. Rev. **2015**, *44*, 4743.

[16] T. Brunhes, P. Boucaud, S. Sauvage, A. Lemaître and J.-M. Gérard, F. Glotin, R. Prazeres, and J.-M. Ortega, Phys. Rev. B **2000**, *61*, 5562.

[17] S. Sauvage, P. Boucaud, T. Brunhes, F. Glotin, R. Prazeres, J. M. Ortega, and J. M. Gérard, Phys. Rev. B **2001**, *63*, 113312.

[18] M. Zielinski, D. Oron, D. Chauvat, and J. Zyss, Small **2009**, *5*, 2835.

[19] C. M. Duque, M. E. Mora-Ramos, and C. A. Duque, J. Nanopart. Res. **2011**, *13*, 6103.

[20] J.C. Martínez-Orozco, M.E. Mora-Ramos, C.A. Duque, J. Photoluminescence **2012**, *132*, 449.

[21] M. R. Singh, Nanotechnology **2013**, *24*, 125701.

[22] C. M. Duque, M. E. Mora-Ramos, and C. A. Duque, J. Photoluminescence **2013**, *138*, 53.

[23] D. Turkpence, G. B. Akguc, A. Bek, and M. E. Tasgin, J. of Optics **2014**, *16*, 105009.

[24] Y. B. Yu, S. N. Zhu, and K.X. Guo, Phys. Lett. A **2005**, *335*, 175.

[25] S. Baskoutas, E. Paspalakis, and A. F. Terzis, Phys. Rev. B **2006**, *74*, 153306.

[26] S. Baskoutas, E. Paspalakis, and A. F. Terzis, Journal of Physics: Condensed Matter **2007**, *19*, 395024.

[27] N. Baer, S. Schulz, P. Gartner, S. Schumacher, G. Czycholl, and F. Jahnke, Phys. Rev. B **2007**, *76*, 075310.

[28] J. Flórez and A. Camacho, Nanoscale Res. Lett. **2011**, *6*, 268.

[29] H. Y. Ramirez, A. S. Camacho, and L. C. Lew Yan Voon, J Phys: Condens. Matter **2007**, *19*, 346216.

[30] N. R. Fino, A. S. Camacho, and H. Y. Ramírez, Nanoscale Res. Lett. **2014**, *9*, 297.

[31] J. S. Ross, S. F. Wu, H. Y. Yu, N. J. Ghimire, A. M. Jones, G. Aivazian, J. G. Yan, D. G. Mandrus, D. Xiao, W. Yao, and X. D. Xu, Nature Comm. **2013**, **4**, 1474.

[32] Y. R. Shen, *The principles of nonlinear optics*, Wiley-Interscience, Hoboken NJ, USA **2003**. Chapters 2 and 7.

[33] R. W. Boyd, *Nonlinear Optics*, 3rd Ed., Academic Press, Burlington MA, USA **2008**, Chapter 1.

[34] E. Rosencher, and Ph. Bois, Phys. Rev. B **1991**, *44*, 11315.

[35] A. Muller, E. B. Flagg, P. Bianucci, X. Y. Wang, D. G. Deppe, W. Ma, J. Zhang, G. J. Salamo, M. Xiao, and C. K. Shih, Phys. Rev. Lett. **2007**, *99*, 187402.

[36] Z. Zeng, A. Petoni, C. S. Garoufalis, S. Baskoutas, and G. Bester, Phys. Chem. Chem. Phys. **2015**, *17*, 1197.

[37] W. Que, Phys. Rev. B **1992**, *45*, 11036.

[38] W. D. Sheng, S. J. Cheng, and P. Hawrylak, Phys. Rev. B **2005**, *71*, 035316.

[39] H. Y. Ramirez, C. H. Lin, C. C. Chao, Y. Hsu, W. T. You, S. Y. Huang, Y. T. Chen, H. C. Tseng, W. H. Chang, S. D. Lin, and S. J. Cheng, Phys. Rev. B **2010**, *81*, 245324.

[40] Arthur J. Nozik, Chem. Phys. Lett. **2008**, *457*, 3.

[41] Y. He, Y.-M. He, J. Liu, Y.-J. Wei, H. Y. Ramírez, M. Atatüre, C. Schneider, M. Kamp, S. Höfling, C.-Y. Lu, and J.-W. Pan, Phys. Rev. Lett. **2015**, *114*, 097402.

[42] R. J. Warburton, C. S. Dürr, K. Karrai, J. P. Kotthaus, G. Medeiros-Ribeiro, and P. M. Petroff, Phys. Rev. Lett. **1997**, *79*, 5282.

[43] W. Xie, Phys. Status Solidi B **2009**, *246*, 2257.

[44] J. Flórez, A. Camacho, and H. Y. Ramírez, Phys. Status Solidi B **2012**, *249*, 2150.

[45] H. Kosaka, A. A. Kiselev, F. A. Baron, Ki Wook Kim, and E. Yablonovitch, Electronic Letters **2001**, **37**, 464.

[46] G. Medeiros-Ribeiro, E. Ribeiro, H. Westfahl Jr., Applied Physics A **2003**, *77*, 725.

[47] W. D. Sheng, S. J. Xu, and P. Hawrylak, Phys. Rev. B **2008**, *77*, 241307(R).

[48] Y. T. Chen, S. J. Cheng, and C. S. Tang, Phys. Rev. B **2010**, *81*, 245311.

[49] M. Bayer, G. Ortner, O. Stern, A. Kuther, A. A. Gorbunov, A. Forchel, P. Hawrylak, S. Fafard, K. Hinzer, T. L. Reinecke, S. N. Walck, J. P. Reithmaier, F. Klopf, and F. Schfer, Phys. Rev. B **2002**, *65*, 195315.

[50] R. M. Stevenson, R. J. Young, P. Atkinson, K. Cooper, D. A. Ritchie, and A. J. Shields, Nature (London) **2006**, *439*, 179.

[51] Along this work, the following InGaAs/GaAs quantum dot parameters were used: $l_r^e = 4.8$nm , $l_z^e = 1.9$nm , $\varepsilon = 14.5$, $m_e^* = 0.04m_e$, $m_h^* = 0.5m_e$, and a strained bandgap of 900 meV.

[52] H. Y. Ramírez and A. Santana, Comp. Phys. Comm. **2012**, *183*, 1654.

[53] For the optical calculation parameters, to ease comparison we use the same as those in reference [16]; i.e. $n_0 = 8\times10^{23}$ and $\Gamma_{12} = \Gamma_{12} = 0.2$ meV. Our calculated susceptibility $\chi^{(2)}_{2\omega}$ corresponds to $\chi^{(2)}_{zzz}$ there

[54] T. Brunhes, P. Boucaud, S. Sauvage, F. Glotin, R. Prazeres, J. M. Ortega, A. Lemaître and J. M. Gérard, Appl. Phys. Lett. **1999**, *75*, 835.

[55] Effects of these two aspects, in first approximation, may be expected to compensate each another so that sparing comparison is reasonable.

[56] F. Vasko and A. Kuznetsov, *Electronic States and Optical Transitions in Semiconductor Heterostructures*, Springer-Verlag, New York NY, USA *1999*. Chapter 3.

[57] The calculated values for z_{31} in the cases of non interacting e-h were not exactly zero, although more than ten orders of magnitude smaller than the ones obtained when the Coulomb interaction was turned on. This because they were computed by numerical integration over a finite domain which was not completely symmetrical as consequence of the shift generated by the bias field. Thus, those tiny numbers were considered spurious.

[58] W. Xie, Phys. Status Solidi B **2012**, *249*, 2153.

[59] R. J. Warburton, C. Schulhauser, D. Haft, C. Schäflein, K. Karrai, J. M. Garcia, W. Schoenfeld, and P. M. Petroff, Phys. Rev. B **2002**, *65*, 113303.

[60] M. F. Tsai, H. Lin, C. H. Lin, S. D. Lin, S. Y. Wang, M. C. Lo, S. J. Cheng, M. C. Lee and W. H. Chang, Phys. Rev. Lett. **2008**, *101*, 267402.

[61] For the i-th state, in the X^0 case the Coulomb diagonal correction is given by $\mid V^i_{eh} \mid$, while in the X^- case it is given by $\mid 2V^i_{eh} - V^i_{ee} \mid < \mid V^i_{eh} \mid$ because $\mid V^i_{ee} \mid$ does not depend on the bias field.